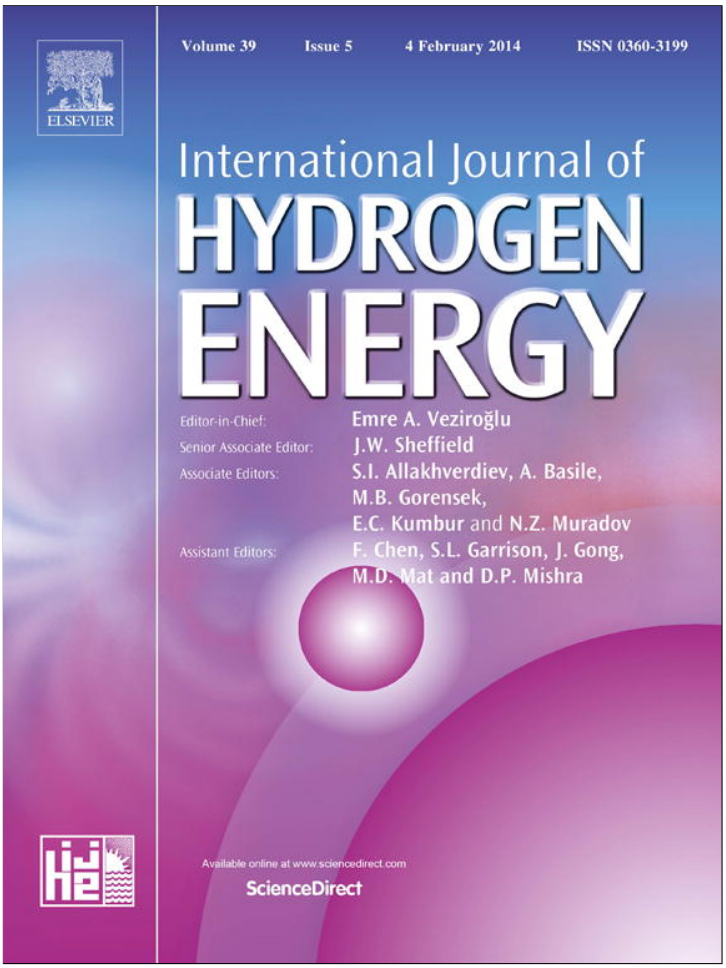

INTERNATIONAL JOURNAL OF HYDROGEN ENERGY 39 (2014) 2160–2167

Available online at www.sciencedirect.com

ScienceDirect

journal homepage: www.elsevier.com/locate/he

Enhanced room-temperature hydrogen storage capacity in Pt-loaded graphene oxide/HKUST-1 composites

Hu Zhou [a,b], *Xiaoqing Liu* [c], *Jun Zhang* [c], *Xiufen Yan* [c], *Yuanjun Liu* [c], *Aihua Yuan* [c,*]

[a] *School of Material Science and Engineering, Jiangsu University of Science and Technology, Zhenjiang 212003, PR China*

[b] *SiYang Diesel Engine Manufacturing Co., Ltd, Zhenjiang 212003, PR China*

[c] *School of Biology and Chemical Engineering, Jiangsu University of Science and Technology, Zhenjiang 212003, PR China*

ARTICLE INFO

Article history:
Received 24 September 2013
Received in revised form
16 November 2013
Accepted 26 November 2013
Available online 30 December 2013

Keywords:
Metal-organic frameworks
Graphene oxide
Pt
Composites
Hydrogen storage
Spillover

ABSTRACT

Series of Pt-loaded graphene oxide (GO)/HKUST-1 composites were synthesized by the reaction between Pt@GO and precursors of HKUST-1. The parent materials and composites have been characterized by powder X-ray diffraction (XRD), Infrared (IR) spectroscopy, scanning electron microscopy (SEM), transmission electron microscopy (TEM), energy dispersive spectroscopy (EDS), and gas adsorption analyzer. The XRD and IR analysis showed that the incorporation of Pt@GO did not prevent the formation of HKUST-1 units. SEM, TEM and EDS results revealed that Pt nanoparticles were well-dispersive and anchored tightly into composites. Meanwhile, the percentage of Pt@GO has an obvious effect on morphologies, crystallinities and surface areas of composites. More importantly, the significant enhancement of hydrogen storage capacity at ambient temperature for the composite with low Pt@GO content can be ascribed to the hydrogen spillover mechanism in such system.

1. Introduction

Metal-organic frameworks (MOFs) have been proven to be a very promising candidate in the field of gas separation and storage because of their extremely large surface areas and porosities, adjustable pore sizes, high thermal and chemical stabilities [1]. Great efforts have been dedicated to search for MOFs with high hydrogen storage capacities in the past few years and significant improvement has been achieved [2]. Unfortunately, these high adsorption amounts were measured only at 77 K and declined dramatically at ambient temperature, due to the weak physisorption of hydrogen on MOFs. For example, the capacities for MOF-5 and HKUST-1 are well below 0.4 wt% at 298 K and 65 bar, although both materials are claimed to have very high surface areas and hydrogen uptakes at 77 K [3].

* *Corresponding author*. Tel.: +86 511 85638920.
E-mail address: aihuayuan@163.com (A. Yuan).

0360-3199/$ – see front matter
http://dx.doi.org/10.1016/j.ijhydene.2013.11.109

The hydrogen spillover, generally defined as the diffusion of dissociated hydrogen on a metal catalyst and subsequent migration of atomic hydrogen to the support surface, has provided a promising route to improve significantly hydrogen storage capacities at ambient temperature of sorbents [4]. Enhancing the contact between the source and receptor is very crucial to facilitate the spillover process and hence increase hydrogen adsorption amounts [5]. Recently, by physically mixing 5 wt% Pt on active carbon (AC) with MOF and then building the carbon bridge between them, the secondary spillover was facilitated significantly. The hydrogen uptakes at 298 K of bridged-IRMOF-1 and IRMOF-8 have been improved greatly compared to those of unbridged-MOFs [6,7]. Similarly, the enhancement of hydrogen storage capacities was also observed on bridged-MOF-177 [8], MIL-101 and MIL-53 [9,10]. Unfortunately, the reproducibility of hydrogen spillover enhancement by above bridge-building method was affected by many factors, including contacts between the dissociation source and receptor, metal particle sizes and doping method, etc [11–13]. To maximize the spillover enhancement was highly empirical and difficult to achieve.

As we all know, graphene oxide (GO) with rich functional groups is very suitable to construct graphene-based hybrid composites [14]. Petit and Bandosz have reported the formation of GO/MOF composites via interactions between oxygen groups of GO and metallic centers of MOF, where the synergetic effect between MOF units and GO layers was responsible for enhanced adsorption amounts compared to the parent material [15–18]. Recently, the nanosized HKUST-1 and ZIF-8 were induced by the incorporation of GO component. The carbon dioxide and hydrogen adsorption capacities of composites have been greatly improved owing to the synergetic effect of both components [19,20].

Combining the merits of GO/MOF composites and hydrogen spillover mechanism, series of Pt-loaded GO/HKUST-1 hybrid composites were prepared in this contribution through in-situ synthesis method, by the reaction between Pt@GO and precursors of HKUST-1. The present contribution can provide further insights into the properties of hybrid composites and the phenomenon of hydrogen spillover, although platinum is a highly expensive metal and its incorporation in porous materials for hydrogen storage has limited practical interest. To our knowledge, the syntheses and characterizations of Pt@GO/MOF hybrid composites were not reported to date, although several GO/MOF composites have been documented. Unlike high uncertainty of the MOF-bridging technique, doping nanoparticles through in-situ synthesis method into GO/MOF units exhibits more controllable and reliable synthesis procedure. More interesting is that the hydrogen adsorption capacity at ambient temperature of the composite with low Pt@GO proportion has been improved significantly, due to the presence of spillover mechanism.

2. Experimental

2.1. Synthesis

Unless otherwise mentioned, all reactants were used as purchased without further purification.

2.1.1. Graphene oxide

Graphene oxide was prepared from the natural flake graphite purchased from Qingdao Guyu Graphite Co., Ltd., with a particle size of 150 μm (99.9% purity) according to a modified Hummers method [21]. In a typical synthesis, graphite (2.0 g) was added to cold (0 °C) concentrated H_2SO_4 (80 mL) in an ice bath. Then, $NaNO_3$ (4.0 g) and $KMnO_4$ (8.0 g) were added gradually under stirring and the temperature of the mixture was kept to be below 10 °C. The reaction mixture was continually stirred for 4 h below 10 °C. Successively, the mixture was stirred at 35 °C for 4 h, and then diluted with deionized (DI) water (200 mL). Because the addition of water in concentrated sulfuric acid medium releases a large amount of heat, the addition of water was performed in an ice bath to keep the temperature below 100 °C. After adding all DI water, the mixture was stirred for 1 h. The reaction was then terminated by adding 30% H_2O_2 solution (15 mL). The solid product was separated by centrifugation, washed repeatedly with 5% HCl solution until sulfate could not be detected with $BaCl_2$. For further purification, the resulting solid was redispersed in DI water and then was dialyzed for 3 days to remove residual salts and acids. The suspension was dried in a vacuum oven at 60 °C for 24 h to obtain graphene oxide (GO).

2.1.2. Pt@GO

Pt particles were introduced onto the GO surface using a well-known chemical reduction method [22]. As-synthesized GO (50 mg) was dispersed in DI water (50 mL) by sonication for 30 min to form stable GO colloid. The ethylene glycol (100 mL) and DI water solution (2.5 mL) of H_2PtCl_6 (0.01 M) were added to the solution with magnetic stirring for 30 min. Then the mixture was put in an oil bath and heated at 100 °C for 6 h with magnetic stirring. The products were separated from the ethylene glycol solution in the centrifuge, washed with DI water three times, and dried in an oven at 60 °C for 12 h. The Pt-loaded GO sample was named as PG.

2.1.3. HKUST-1

Typically, $Cu(NO_3)\cdot 5H_2O$ (2 g) and 1,3,5-benzenetricarboxylic acid (BTC) (1 g) were dissolved in N,N′-dimethylformamide (DMF, 17 mL), and the mixture was stirred for 5 min at room temperature. Ethanol (17 mL) and DI water (17 mL) was added to the mixture and then stirring and sonication for 30 min were performed. The mixture was then transferred to an 80 mL Teflon-line stainless-steel vessel and heated to 100 °C at a rate of 10 °C h^{-1} and kept at this temperature for 4 h. After cooling, the crystals were filtered, washed and immersed in dichloromethane. Dichloromethane was changed twice during three days. The crystals were collected after filtration and washing with dichloromethane. Drying was then performed by heating the crystals at 180 °C under vacuum for 28 h. The resulting product was kept in a dessicator and referred as HPG0.

2.1.4. Pt@GO/HKUST-1 composites

The composites were prepared in the same procedure as HKUST-1 except that various amounts of PG were added to the mixture of HKUST-1 precursors before the heat treatment. The added GO consisted of 5 and 10 wt% of the final material weight. The composites are referred as HPG5 and HPG10,

respectively. It should be pointed out here that the same experimental conditions were employed to avoid the variability in the properties of our materials (HPG0, HPG5 and HPG10) between batches during samples syntheses. Three autoclaves containing precursors of HPG0, HPG5 and HPG10 were all put into the same oven at the same time, and then the identical temperature procedure and subsequent processing were carried out for these autoclaves. So we believe that three samples in our case are products of the same batch and the difference in the properties between them can be reasonably ascribed to the incorporation of PG component.

2.2. Instrumentation and measurements

Powder X-ray diffraction (XRD) patterns were collected on a Shimadzu XRD-6000 diffractometer with CuK_α ($\lambda = 0.1543$ nm) radiation at a scan speed of 4° min^{-1}. IR spectra were measured on a Nicolet FT 1703X spectrophotometer in the 4000–400 cm^{-1} region (KBr pellets). The morphology and structure of products were examined by the scanning electron microscope (SEM, JEOL JSM-6480) and transmission electron microscopy (TEM, JEOL JEM-2100). The compositions of products were determined by energy-dispersive X-ray spectrometry (EDS, Oxford INCA). Low-pressure nitrogen (77 K) and hydrogen (77 K and 298 K) adsorption isotherms were performed using an ASAP 2020 instrument (Micromeritics). High-pressure hydrogen adsorption measurements at 298 K were measured gravimetrically using a high resolution magnetic suspension balance sorption device (ISOSORP-HyGra+V, Rubotherm). Approximately 150 mg of HPG0 and composites were heated to 180 °C with a rate of 2 °C min^{-1} and outgassed at 180 °C for 24 h. The GO and PG samples were outgassed at 80 °C. UHP grade N_2 and H_2 (99.999%) gases were used for all measurements.

3. Results and discussion

3.1. Powder XRD patterns

Powder XRD patterns of the parent materials and composites are shown in Fig. 1 and Fig. S1 (Supplementary material). An obvious diffraction peak (002) observed for GO at $2\theta = 9.76°$ (Fig. S1) are ascribed to the introduction of oxygen-containing functional groups on the graphite sheet surfaces [23]. The interlayer spacing of 0.91 nm determined by Bragg's law is much larger than that of pristine graphite (approximately 0.34 nm) [24]. For the PG material, the diffraction peaks at $2\theta = 39.6$, 46.2, 67.4 and 81.4 can be assigned to the characteristic (111), (200), (220) and (311) crystalline planes of face-centered-cubic Pt, respectively. The XRD pattern of HPG0 was agreement with that reported in the literature [25,26], demonstrating a successful synthesis procedure. It is interesting to notice that the diffraction patterns of both composites were similar to that observed for the parent HPG0, indicating that the well-defined MOF structure has been preserved and the incorporation of PG component did not prevent the formation of linkages between copper dimers and BTC bridges. It should be noted here that the intensity of diffraction peaks for composites decreased with increasing PG content from 5 to 10 wt%. The much low intensity observed in HPG10 is related to the low crystallization caused by the incorporation of PG with high content. On one hand, the functional oxygen groups from excessive PG flakes react with copper sites to form uniform new structures. One the other hand, the PG component suspended in the reaction mixture may act as a nucleation surface, promoting the formation of very small MOF crystallites. However, the characteristic peaks of PG were not observed in both composites, owing to the following two reasons: 1) the low intensity and broad peaks of PG were swamped by high intensity and sharp peaks of HPG0, as well as relatively low PG contents in composites; 2) the GO sheets readily exfoliated/dispersed in ethanol/water upon sonication during composites syntheses [27].

3.2. IR spectra analysis

IR spectra of GO has been described in detail elsewhere and the vibration peaks are consistent with fingerprint groups (Fig. S2) [22,28]. After incorporation of Pt metals, the absorption band of carboxyl groups for PG at around 1700 cm^{-1} is observable but not as prominent as that observed for GO. The vibration bands related to functional groups of PG in composites are not seen, due to the rather low intensity

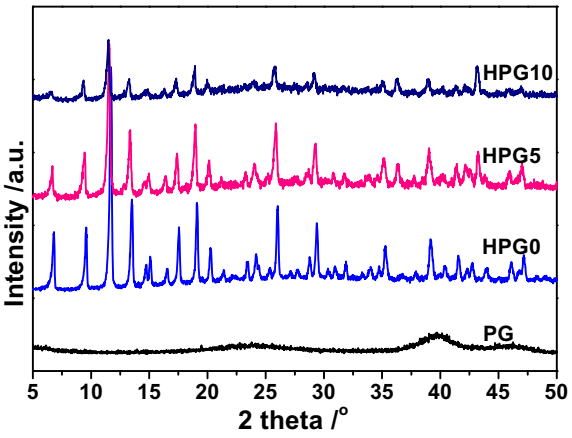

Fig. 1 – Powder XRD patterns of the parent materials and composites.

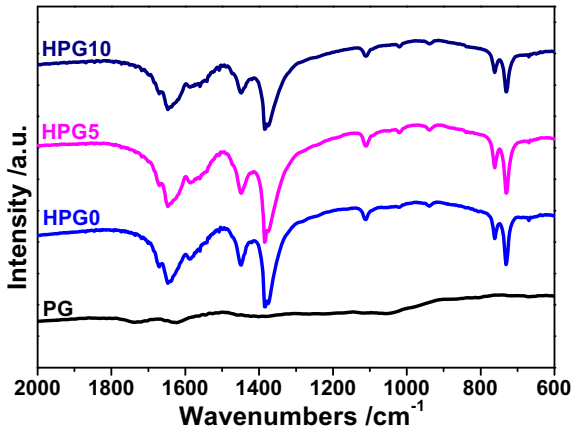

Fig. 2 – IR spectra of the parent materials and composites in the region of 2000–600 cm^{-1}.

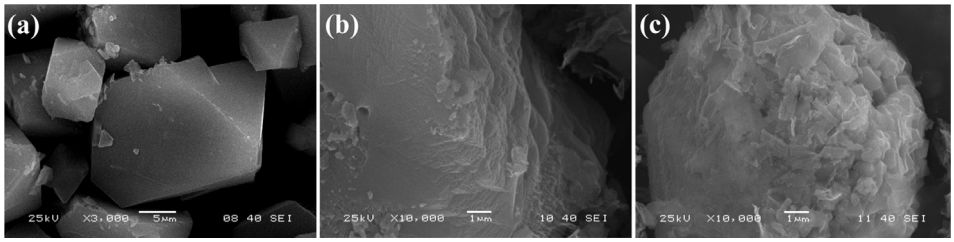

Fig. 3 – SEM images of (a) HPH0, (b) HPG5 and (c) HPG10.

adsorption peaks and the low PG content (Fig. 2). It should be noticed that IR spectra of HPG0 and both composites exhibit similar bands, characteristic features of HKUST-1 [29]. The symmetric and asymmetric stretching vibrations of carboxylate groups in BTC appear at 1645/1590 cm^{-1} and 1450/1370 cm^{-1}, respectively. The lower wavenumber region of 1300–700 cm^{-1} exhibits various bands assigned to out-of-plane vibrations of BTC. Above analysis is indicative of the coordination of BTC to the copper sites, and the incorporation of PG did not prevent the formation of MOF units. The decrease in the intensity of bands can be noticed in HPG10, which may be related to the low HPG0 content in the composite. Above analysis is in accordance with the results draw from XRD experiments.

3.3. *Morphological analysis*

The visible color change of composites was observed with the introduction of PG component. Both composites changed a much darker green than HPG0, as shown in Fig. S3. The change in the color for composites indicated that PG is well incorporated into the parent material.

The heterostructure of materials can be verified by the morphological analyses. The SEM images showed that GO was seen as dense agglomerates of sheets stacked together by dispersive forces (Fig. S4). We can see from Fig. S5 that the Pt nanoparticles are well-dispersed on the GO surface and no apparent aggregation can be observed. Element mapping image and EDS spectrum of PG also confirmed the presence of homogeneously distributed Pt metals through the GO sheets with Pt content of 18.9 wt% (Fig. S6). In addition, the presence of characteristic peaks of oxygen element indicated functional oxygen groups were still reserved on GO layers after doping Pt metals. The pristine material HPG0 shows typical octahedral crystalline shapes with some defects [26] (Fig. 3a). In contrast, the structure of composites show some variations compared to the one of HPG0. The layered structure in HPG5 is quite similar to the ones found in MOF-5/GO and HKUST-1/GO composites [15,18] (Fig. 3b). In the structure of HKUST-1/GO composites, the layers have been confirmed as the alternation between GO sheets and HKUST-1 blocks, where the functional oxygen groups from GO interact with the copper dimmers and chemical interactions are involved in the formation of composites. Similarly, these layered morphology observed in our case (HPG5) is also indicative of intercalations of PG layers and MOF blocks, and there are interactions between the oxygen groups from PG and the copper dimers. Separate agglomerates with stacked PG layers are found with increasing GO ratio in the composite (Fig. 3c). In fact, this part of PG did not interact with the MOF units and was responsible for the obvious decrease in porosity of the HPG10 composite.

It is well known that HPG0 is extremely sensitive to the electron beam and the structure could collapse after a few minutes [30]. However, the lattice images of HPG0 crystals were observed successfully in our materials. This can be attributed to the fact that the incorporated PG component retained the crystalline structure of HKUST-1 by dissipating electrostatic charges, as observed in the MOF-5/CNTs composite [31]. For the HPG5 composite, the dark spots of Pt metals with particle size of about 3.5 nm are well-dispersed on the GO layers embedded with HPG0 units (Fig. 4a). It is noticeable that agglomerates with stacked distorted graphene-based layers are observed in HPG10. In addition, the lattice image of HPG0 appeared (Fig. 4b), similar to that found in the GO/HKUST-1

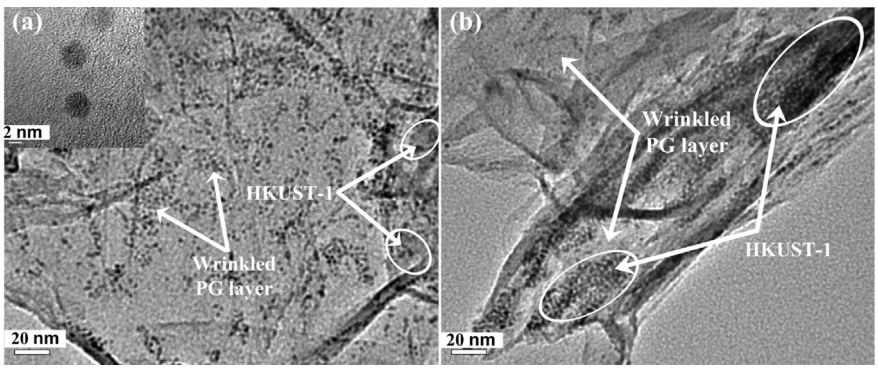

Fig. 4 – HRTEM images of (a) HPG5 and (b) HPG10, in which the wrinkled PG layers, crystals or lattice images of HKUST-1 are shown and indicated by arrows.

composite [18]. It should be noted here that only the ratios of the added GO component in the final materials before the heat treatment were shown for all GO/MOF composites reported in literatures [15,17–20], and the actual contents of GO in as-synthesized composites are not determined owing to the extreme difficulties. Similarly, the definitive content of PG in our composites can also not be given, based on structural complexities of such system and the fact that both oxygen and carbon elements are involved in two components (PG and MOF). Considering above reasons, EDS analyses of HKUST-1 and composites were carried out to roughly assume the content of Pt in composites, as listed in Table S1. The contents of Pt were evaluated based on the maps of elements collected from four spots. The increase of PG component in composites has been confirmed by the increase in the percentage of Pt (from 1.46 wt% in HPG5 to 3.38 wt% in HPG10). Furthermore, the element maps show that C, O, Cu and Pt are well-dispersed on a larger scale of ~300 microns (Figs. S6–S8), suggesting that PG and MOF components in composites are well mixed throughout the whole samples. Simultaneously, element mapping images of both composites at a small scale (~6 microns) (Figs. S9 and S10) also indicate that these elements are uniformly dispersed in the micro/nano region. This result is well consistent with that observed from SEM and TEM images.

3.4. *Textural characterization*

Textural parameters of materials were evaluated from nitrogen adsorption measurements at 77 K (Fig. 5). PG exhibited a significantly low and negligible porosity. The parent material HPG0 and both composites exhibit a type-I isotherm with a hysteresis loop at relative pressure from 0.45, indicating the predominant microporous character of such materials. The hysteresis loop observed for HPG0 suggests the presence of mesopores between small MOF crystals, while the loops found for both composites might be caused by the larger pores between composites particles, as well as at the interface between GO flakes and MOF units. As shown in Table S2, the V_{meso}/V_{tot} ratio of samples increases from 0.19 (HPG0) to 0.36 (HPG10) via 0.33 (HPG5) upon increasing the PG content. The BET surface area of 937 $cm^2\ g^{-1}$ for HPG0 is in the range of values reported previously [25,32,33]. The BET values of composites decrease from 848 $cm^2\ g^{-1}$ (HPG5) to 676 $cm^2\ g^{-1}$ (HPG10) with the increase of PG content. An obvious decrease observed in the HPG10 composite can be ascribed to the following facts: 1) the pore volume of HPG10 is reduced by high-content PG with much low porosity; 2) the introduction of excessive PG caused low crystallization of products, which has been confirmed by decreased intensities of XRD peaks for HPG10; 3) excessive PG flakes in the HPG10 composite remain as agglomerates, which caused the obvious reduction of the total pore volume of 0.45 $cm^3\ g^{-1}$, compared to 0.53 $cm^3\ g^{-1}$ of HPG0.

3.5. *Hydrogen storage capacities*

Low-pressure hydrogen adsorption measurements of the parent materials and composites were carried out at 77 K and 1.1 bar. As shown in Fig. 6, PG has a negligible adsorption capacity of 0.2 wt% comparable to 1.8 wt% for HPG0. The HPG10 composite exhibited a notable decrease in hydrogen storage capacity because of the significantly low surface area. The adsorption uptake of HPG5 was identical to that of HPG0 in spite of some loss in surface area caused by the incorporation of PG component. It is noteworthy that the value measured for HPG5 is higher than the "hypothetical" one (Fig. 7). The latter ones were calculated assuming the physical mixture of the composite components PG and HKUST-1 alone, taking into account the percentage of each component in composites. This result can be ascribed reasonably to the presence of spillover mechanism, which enhances the hydrogen adsorption capacity. As we all know, hydrogen spillover onto MOFs sorbents has been documented recently by several groups via direct doping of nanoparticles (Pt, Pd) [34–39], physical mixing with Pt/AC or Pt/C catalyst [6,7,9,13,40,41], and in-situ loading of Pt/MWCNTs [42]. The metal particles in these systems act as the spillover source of hydrogen molecules and MOFs act as the receptors. The review by Yang and coworkers has provided tremendous insights into the physical properties of hydrogen spillover, a detailed investigated into related MOFs, and guidance on how to improve hydrogen capacities of current MOFs [4]. Furthermore, several computational studies have also shed light onto the phenomenon hydrogen spillover of MOFs [43,44]. As already observed for above systems, Pt

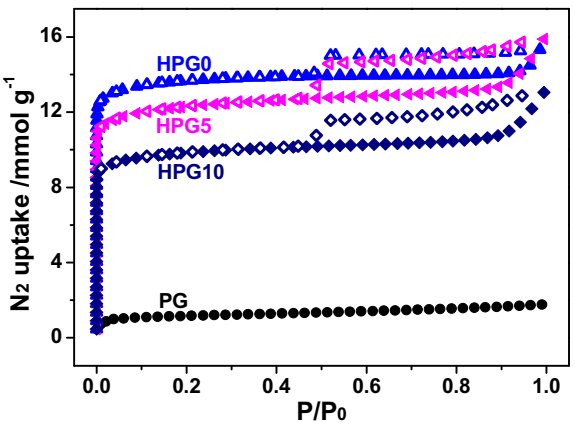

Fig. 5 – Nitrogen adsorption isotherms of the parent materials and the composites at 77 K.

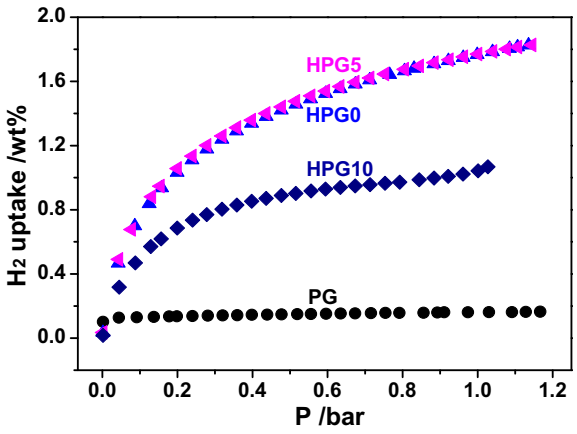

Fig. 6 – Low-pressure hydrogen adsorption isotherms at 77 K of the parent materials and composites.

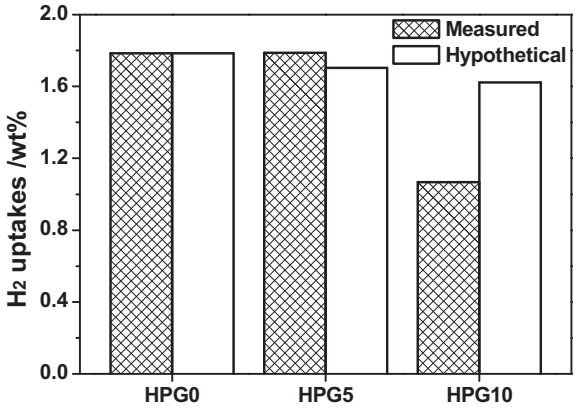

Fig. 7 – Measured and "hypothetical" hydrogen storage capacities at 77 K and 1.0 bar of the pristine material and composites.

nanoparticles involved in our composites undoubtedly act as the hydrogen spillover source. In our system, more intimate contacts between Pt particles and GO/HKUST-1 receptor have led to a lower energy barrier for the spillover of dissociated hydrogen from Pt to the receptor, as observed in Pt/C materials [5]. As a result, hydrogen molecules first chemisorbed and dissociated on the surface of Pt and then migrated to the surface of the primary spillover receptor GO. Subsequently, hydrogen atoms further diffuse into the second spillover receptor HKUST-1 with high porosity and new pores at the interface between GO layers and HKUST-1 units.

For the high-pressure hydrogen adsorption measurements at 298 K, (Fig. 8) the storage capacity (0.41 wt%) at 80 bar of HPG0 was higher than ~0.27 wt% reported in the literature under the same condition [10]. For the HPG10 composite, the obvious decrease of hydrogen adsorption capacity induced by the low surface area has offset the enhancement caused by spillover effect. Surprisingly, a remarkably high hydrogen uptake of 0.77 wt% at 80 bar is noticed for HPG5 compared to HPG10 (0.15 wt%) and HPG0 (0.41 wt%). In fact, the hydrogen storage capacity at 298 K observed in HPG5 is higher obviously

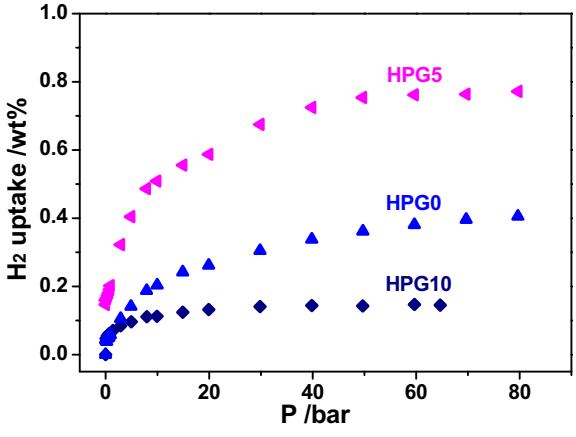

Fig. 8 – High-pressure hydrogen adsorption isotherms at 298 K of HPG0 and composites.

than 0.28 wt% (65 bar) for MOF-5 [3] and 0.43 wt% (80 bar) for MIL-101 [45]. This phenomenon was also found in the Pt-loaded MWCNTs@MOF-5 composites [42]. The hydrogen storage capacity at 298 K and 100 bar was enhanced 4.2 times higher than that of pure MOF-5 upon the incorporation of Pt-MWCNTs, which was caused by the presence of spillover effect. The 1.9-fold enhancement in HPG5 indicates that the spillover has played an important role in terms of hydrogen storage at the ambient temperature. Notably, considering the fact that Pt nanoparticles exhibit high catalytic activities at evaluated temperatures (vs 77 K), the spillover effect at 77 K observed in our case is not significant compared to that at 298 K. Low-pressure hydrogen adsorption experiments at 298 K were also carried out and the isotherms of these materials are shown in Fig. S11, in which the HPG5 composite has a higher uptake than HPG0 and HPG10. So the low-pressure adsorption trend at 298 K is well consistent with that observed from the high-pressure adsorption result. Furthermore, the powder XRD patterns of HPG0 and both composites after hydrogen adsorption experiments were performed to assess the effect of outgassing on materials. As shown in Fig. S12, the XRD patterns of the activated samples are well agreement with those of as-synthesized products, indicating the higher thermal stability and permanent porosity of such system.

4. Conclusions

In this work, series of Pt-loaded GO/HKUST-1 hybrid composites were prepared via in-situ synthesis method, in which Pt nanoparticles were well-dispersive and anchored tightly into GO/MOF units. The composites remained the same structure as the parent HKUST-1, while the morphologies and texture parameters of composites were induced obviously by the Pt@GO ratio. The nearly twofold increase in hydrogen uptake at 298 K observe in HPG5 compared to HKUST-1 can be reasonably attributed to the spillover mechanism and the high porosity of the secondary receptor HKUST-1. Furthermore, the imitate contact between the dissociation Pt metal and receptor is an important factor affecting the spillover process. The present work provides useful information for future optimization of Pt-loaded GO/MOF as new type of hydrogen storage candidate materials.

Acknowledgements

The work is supported by the National Natural Science Foundation of China (51072072, 51102119, 51272095), Natural Science Foundation of Jiangsu Province of China (BK2011518).

Appendix A. Supplementary data

Supplementary data (Figs. S1–S12, Tables S1 and S2) associated with this article can be found, in the online version, at http://dx.doi.org/10.1016/j.ijhydene.2013.11.109.

REFERENCES

[1] Furukawa H, Cordova KE, O'Keeffe M, Yaghi OM. The chemistry and applications of metal-organic frameworks. Science 2013;341:1230444.

[2] Sculley J, Yuan DQ, Zhou HC. The current status of hydrogen storage in metal-organic frameworks – updated. Energy Environ Sci 2011;4:2721–35.

[3] Panella B, Hirscher M, Pütter H, Müller U. Hydrogen adsorption in metal-organic frameworks: Cu-MOFs and Zn-MOFs compared. Adv Funct Mater 2006;16:520–4.

[4] Wang LF, Yang RT. New sorbents for hydrogen storage by hydrogen spillover – a review. Energy Environ Sci 2008;1:268–79.

[5] Wang Z, Yang RT. Enhanced hydrogen storage on Pt-doped carbon by plasma reduction. J Phys Chem C 2010;114:5956–63.

[6] Li YW, Yang RT. Significantly enhanced hydrogen storage in metal-organic frameworks via spillover. J Am Chem Soc 2006;128:726–7.

[7] Li YW, Yang RT. Hydrogen storage in metal-organic frameworks by bridged hydrogen spillover. J Am Chem Soc 2006;128:8136–7.

[8] Li YW, Yang RT. Gas adsorption and storage in metal-organic framework MOF-177. Langmuir 2007;23:12937–44.

[9] Liu YY, Zeng JL, Zhang J, Xu F, Sun LX. Improved hydrogen storage in the modified metal-organic frameworks by hydrogen spillover effect. Int J Hydrogen Energy 2007;32:4005–10.

[10] Li YW, Yang RT. Hydrogen storage in metal-organic and covalent-organic frameworks by spillover. AJChE J 2008;54:269–79.

[11] Luzan SM, Talyzin AV. Hydrogen adsorption in Pt catalyst/MOF-5 materials. Microporous Mesoporous Mater 2010;135:201–5.

[12] Campesi R, Cuevas F, Latroche M, Hirscher M. Hydrogen spillover measurements of unbridged and bridged metal-organic frameworks – revisited. Phys Chem Chem Phys 2010;12:10457–9.

[13] Stucket NR, Wang LF, Yang RT. Characteristic of hydrogen storage by spillover on Pt-doped carbon and catalyst-bridged metal organic framework. Langmuir 2010;26:11963–71.

[14] Dreyer DR, Park S, Bielawski CW, Ruoff RS. The chemistry of graphene oxide. Chem Soc Rev 2010;39:228–40.

[15] Petit C, Bandosz TJ. MOF-graphite oxide composites: combining the uniqueness of graphene layers and metal-organic frameworks. Adv Mater 2009;21:4753–7.

[16] Petit C, Bandosz TJ. Enhanced adsorption of ammonia on metal-organic framework/graphite oxide composites: analysis of surface interactions. Adv Funct Mater 2010;20:111–8.

[17] Petit C, Bandosz TJ. Synthesis, characterization, and ammonia adsorption properties of mesoporous metal-organic framework (MIL(Fe))-graphite oxide composites: exploring the limits of materials fabrication. Adv Funct Mater 2011;21:2108–17.

[18] Petit C, Burress J, Bandosz TJ. The synthesis and characterization of copper-based metal-organic framework/graphite oxide composites. Carbon 2011;49:563–72.

[19] Liu S, Sun LX, Xu F, Zhang J, Jiao CL, Li F, Li ZB, Wang S, Wang ZQ, Jiang X, Zhou HY, Yang LN, Schick C. Nanosized Cu-MOFs induced by graphene oxide and enhanced gas storage capacity. Energy Environ Sci 2013;6:818–23.

[20] Kumar R, Jayaramulu K, Maji TK, Rao CNR. Hybrid nanocomposites of ZIF-8 with graphene oxide exhibiting tunable morphology, significant CO_2 uptake and other novel properties. Chem Commun 2013;49:4947–9.

[21] Hummers Jr WS, Offeman RE. Preparation of graphitic oxide. J Am Chem Soc 1958;80:1339.

[22] Xu C, Wang X, Zhu JW. Graphene – metal particle nanocomposites. J Phys Chem C 2008;112:19841–5.

[23] Hontoria-Lucas C, López-Peinado AJ, López-González Jde D, Rojas-Cervantes ML, Martín-Aranda RM. Study of oxygen-containing groups in a series of graphite oxides: physical and chemical characterization. Carbon 1995;33:1585–92.

[24] Liu N, Luo F, Wu HX, Liu YH, Zhang C, Chen J. One-step ionic-liquid-assisted electrochemical synthesis of ionic-liquid-functionalized graphene sheets directly from graphite. Adv Funct Mater 2008;18:1518–25.

[25] Chui SSY, Lo SMF, Charmant JPH, Orpen AG, Wiliams ID. A chemically functionalizable nanoporous material $[Cu_3(TMA)_2(H_2O)_3]_n$. Science 1999;283:1148–50.

[26] Biemmi E, Christian S, Stock N, Bein T. High-throughput screening of synthesis parameters in the formation of the metal-organic frameworks MOF-5 and HKUST-1. Microporous Mesoporous Mater 2009;117:111–7.

[27] Cai DY, Song M. Preparation of fully exfoliated graphite oxide nanoplatelets in organic solvents. J Mater Chem 2007;17:3678–80.

[28] Petit C, Seredych M, Bandosz TJ. Revisiting the chemistry of graphite oxides and its effect on ammonia adsorption. J Mater Chem 2009;19:9176–85.

[29] Seo YK, Hundal G, Jang IT, Hwang YK, Jun CH, Chang JS. Microwave synthesis of hybrid inorganic-organic materials including porous $Cu_3(BTC)_2$ from Cu(II)-trimesate mixture. Microporous Mesoporous Mater 2009;119:331–7.

[30] Houk RJT, Jacobs BW, Gabaly FE, Chang NN, Talin AA, Graham DD, et al. Silver cluster formation, dynamics, and chemistry in metal-organic frameworks. Nano Lett 2009;9:3413–8.

[31] Yang SJ, Choi JY, Chae HK, Cho JH, Nahm KS, Park CR. Preparation and enhanced hydrostability and hydrogen storage capacity of CNT@MOF-5 hybrid composite. Chem Mater 2009;21:1893–7.

[32] Liu JC, Culp JT, Natesakhawat S, Bockrath BC, Zande B, Sankar SG, et al. Experimental and theoretical studies of gas adsorption in $Cu_3(BTC)_2$: an effective activation procedure. J Phys Chem C 2007;111:9305–13.

[33] Thomas KM. Adsorption and desorption of hydrogen on metal-organic framework materials for storage applications: comparison with other nanoporous materials. Dalton Trans 2009:1487–505.

[34] Gutiérrez I, Díaz E, Ordóñez S. Consequences of cavity size and palladium addition on the selective hydrogen adsorption in isoreticular metal-organic frameworks. Thermochim Acta 2013;567:79–84.

[35] Chen H, Wang LF, Yang J, Yang RT. Investigation on hydrogenation of metal-organic frameworks HKUST-1, MIL-53, and ZIF-8 by hydrogen spillover. J Phys Chem C 2013;117:7565–76.

[36] Wang LF, Stuckert NR, Chen H, Yang RT. Effects of Pt particle size on hydrogen storage on Pt-doped metal-organic framework IRMOF-8. J Phys Chem C 2011;115:4793–9.

[37] Zlotea C, Campesi R, Cuevas F, Leroy E, Dibandjo P, Volkringer C, et al. Pd nanoparticles embedded into a metal-organic framework: synthesis, structural characteristics, and hydrogen sorption properties. J Am Chem Soc 2010;132:2991–7.

[38] Proch S, Herrmannsdörfer J, Kempe R, Kern C, Jess A, Seyfarth L, et al. Pt@MOF-177: synthesis, room-temperature hydrogen storage and oxidation catalysis. Chem Eur J 2008;14:8204–12.

[39] Sado M, Henschel A, Fröde H, Klemm E, Kaskel S. Solution infiltration of palladium into MOF-5: synthesis, physisorption and catalytic properties. J Mater Chem 2007;17:3827–32.

[40] Liu XM, Rather S, Li QX, Lueking A, Zhao YG, Li J. Hydrogenation of CuBTC framework with the introduction of a PtC hydrogen spillover catalyst. J Phys Chem C 2012;116:3477–85.
[41] Lee S, Park S. Effect of platinum doping of activated carbon on hydrogen storage behaviors of metal-organic frameworks-5. Int J Hydrogen Energy 2011;36:8381–7.
[42] Yang SJ, Cho JH, Nahm KS, Park CR. Enhanced hydrogen storage capacity of Pt-loaded CNT@MOF-5 hybrid composites. Int J Hydrogen Energy 2013;35:13062–7.
[43] Wang TY, Zhang QJ, Li BH, Chen H, Chen L. Density functional study of hydrogen spillover on direct Pd-doped metal-organic frameworks IRMOF-1. Int J Hydrogen Energy 2012;37:5081–9.
[44] Miller MA, Wang CY, Merrill GN. Experimental and theoretical investigation into hydrogen storage via spillover in IRMOF-8. J Phys Chem C 2009;113:3222–31.
[45] Latroche M, Surblé S, Serre C, Mellot-Draznieks C, Llewellyn PL, Lee JH, et al. Hydrogen storage in the giant-pore metal-organic frameworks MIL-100 and MIL-101. Angew Chem Int Ed Engl 2006;45:8227–31.